Water in Pores: The Gibbs-Thomson Effect

Water in Pores: The Gibbs-Thomson Effect

Amelia Carolina Sparavigna

Department of Applied Science and Technology, Polytechnic University of Turin, Italy

Email: amelia.sparavigna@polito.it

Abstract

When we have a material in two phases and a surface between them, the material tries to minimize the interface area in order to reduce the excess of associated surface energy. The thermodynamic system reacts minimizing the Gibbs free energy. According to the Gibbs' surface thermodynamics, the Gibbs–Thomson effect arises. This phenomenon is relevant to the shift, with respect to the bulk system, of the melting and freezing temperatures of a confined substance, and it is observed in porous frameworks as a function of pore size. Here, we will consider the literature regarding the Gibbs-Thomson effect as observed for the confinement of water in mesoporous silica, porous carbon materials and biochar. Besides the investigation of temperature shift, we will evidence the researchers' specific interest to the liquid-like interfacial layer which is present between the walls of the pores and the confined phase.

Keywords: Water, Gibbs Thomson Equation, Gibbs Composite Systems Thermodynamics, Melting and Freezing Temperature Depression, Mesoporous silica, Mesoporous carbon, Biochar.

Subject Areas: Materials Science.

Submitted SSRN - February 6, 2023

Introduction

When we have a material in two phases and a surface between them, the material tries to minimize the interface area in order to reduce the excess of associated surface energy (Cantor, 2020). The origin of the surface energy is in the local structure and bonding of atoms and molecules. At the surface, atoms and molecules have a greater energy than that possessed by atoms and molecules in either of the two phases. The system reacts minimizing the Gibbs free energy. Considering two phases α, β and related free energies, when $G_\alpha < G_\beta$, α phase creates an outward pressure, balanced by the surface energy at the interface, so that the difference of free energy is given by (Cantor, 2020):

$$\Delta G = G_\beta - G_\alpha = 2V_m \gamma / r \quad (1),$$

where V_m is the molar volume and r the radius of the α domain, which is spherical to minimize the surface area. γ is the interfacial free energy. (1) is the Gibbs-Thomson equation (Cantor, 2020).

The approach of Gibbs thermodynamics to a two-phase system gives rise to the Gibbs–Thomson effect, which is regarding the shift of melting and crystallization temperatures for a confined material, with respect to the thermodynamic system with a flat interface. Consequently, the Gibbs-Thomson effect is observed in porous materials as a function of the pore size. Here, we will consider the melting and freezing of water in

mesoporous silica particles and in porous carbon materials. Let us remember that mesoporous materials are characterized by a framework of pores the size of which is in the range from 2 nm to 50 nm, according to IUPAC terminology (Fang et al., 2010). Pore size is given by the distance between opposite walls of the pore, that is the diameter in the case of cylindrical pores (Sing, 1991, Salamon, 2014).

Besides the investigation of melting and freezing temperature shift, the study of water adsorption and of the related molecular status in mesoporous materials is important for many applications, ranging from water recycling to fossil fuel extraction, as stressed by Wang et al., 2019. The reason is in the peculiar behavior of the confined solvent molecules, which is influenced by the interactions with the walls of the porous material. Moreover, specific interest is devoted to the liquid-like interfacial layer which is present between the walls of the pores and the confined phase (Wang et al., 2019). The molecules, which are in this layer, might behave differently from the molecules in the core of the pores.

In the following discussion we will propose literature mainly about the Gibbs-Thomson effect and the shift of melting and freezing temperatures for water. The liquid-like layer will be considered too.

Bound water and thermoporometry

In a discussion about phase-change materials in wood (Sparavigna, 2022), we mentioned the article by Nopens et al., 2020, who considered the mesopores in the wood cell walls at dry and wet conditions. Nopens and coworkers remember that, in the literature regarding wood, water has been distinguished as "free water, freezing-bound water and non-freezing bound water" (Nopens et al., 2020, Nakamura et al., 1981). To investigate the porosity of wood cell walls as can be deduced from the differential scanning calorimetry, the researchers used the Gibbs-Thomson effect, remarking that the method has an intrinsic low boundary of 2–3 nm pore size, because no melting of water can be observed below this pore size (reference given by Nopens and coworkers is Park et al., 2006). Park and coworkers give the relation between the pore diameter D and the *depressed melting temperature* $T(D)$, in the following form of the Gibbs–Thomson equation:

$$\Delta T = T_0 - T(D) = -\frac{4 T_0 \gamma_{ls}}{D \rho H_f} \cos\phi \qquad (2)$$

In (2), which is different from the previously given (1), T_0 is the melting temperature of bulk water (273.15 K), γ_{ls} is the surface energy at ice-water interface (12.1 mJ/m^2), ρ, H_f are density and bulk enthalpy of fusion (specific heat of fusion) of freezing bound water, assumed to be equal to that of unbounded water (1000 kg/m^3 , 334 J/g). D is the diameter of the pore. ΔT is the melting temperature depression. Then the water in a *smaller* pore has a *larger* melting temperature depression. Usually, angle ϕ is assumed to be near 180° in cylindrical pores.

In the dimensional form, (2) gives:

$$\left[\frac{k_B \Delta T}{k_B T_0}\right] = \left[\frac{\gamma_{ls}}{D \rho H_f}\right] = \left[\frac{energy \cdot L^{-2}}{L \cdot M \cdot L^{-3} \cdot energy \cdot M^{-1}}\right] = \left[\frac{energy}{energy}\right] \quad ,$$

where k_B is the Boltzmann constant, and M, L are the dimensions of mass and length.

Here, it is better to remember also the expression of the Gibbs-Thomson effect given by Jackson and McKenna, 1990, of the melting point depression for a small spherical crystal (size d) in its own liquid in the form:

$$\Delta T = T_0 - T(d) = \frac{4 T_0 \gamma_{ls}}{d \rho H_f} \qquad (3)$$

It is assumed an isotropic surface energy at solid-liquid interface and that the crystal side is sufficiently large that the material retains its bulk properties for density and specific heat.

Jackson and McKenna investigated the phase transition temperatures and heats of fusion for nonpolar organic materials (cis- and trans-decalin, cyclohexane, benzene, chlorobenzene, naphthalene, heptane) confined in controlled pore glasses. The pore diameter D was in the range of 4–73 nm. As for the previous studies of inorganic materials, the melting point $T(D)$ decreased with decreasing pore diameter. Also a reduction in the bulk enthalpy of fusion was measured.

For what is regarding the study of the pore size distribution in the wood cell wall, a very recent work has been proposed by Zhong and Ma, 2022. The research is based on data provided by differential scanning calorimetry (DSC) thermoporometry, in the framework of a continuous method. "The pore size distribution (PSD) of cell wall is crucial for the wood", and can be analyzed by means of "the heat absorption of cell wall water upon melting" (Zhong & Ma, 2022). For a detailed discussion about the thermoporometry by means of the differential scanning calorimetry, Landry, 2005, is a proper reference (the first method for simultaneous determination of shape and size of pores was proposed in 1977 by Brun et al.). In any case, it is necessary to stress Landry told that "no general consensus for DSC temperature programs [exists], as experimental conditions are often dictated by many variables". The variable are regarding "the characteristics of the porous solid, the solidification temperature of pore-filling liquid, the sample size, the instrument capabilities, and most often, the analyst preferences" (Landry, 2005).

Of course, the importance of the confinement of water is not only relevant for wood. Let us mention just a recent study, that by Salvati Manni et al., 2019. "Water in restricted geometries has different properties than in bulk. Confinement can prevent low-temperature crystallization of the molecules into a hexagonal structure and thus create a state of amorphous water" (Salvati Manni et al., 2019). What is relevant to understand is the "survival of life at subzero temperatures", because of its nanoconfinement into lipidic membranes. In fact, Salvati Manni and coworkers, by means of specifically designed synthetic lipids, were able of maintaining "amorphous water down to ~10 K due to nanoconfinement". Let us note that the system is displaying a lipid–water phase diagram, with the presence of bicontinuous cubic and lamellar liquid crystalline phases, with the presence of "subzero liquid, glassy or ice water".

In an article provided by ETH Zurich, 2019, announcing the results by Salvati Manni and coworkers, it is told that research has "identified an unusual way to prevent water from forming ice crystals". The first step is the design and synthesis of lipids able to produce lipidic mesophases. The lipids are spontaneously self-assembling and aggregating to create membranes, which are assuming the form "a network of connected channels that measure less than one nanometer in diameter" (ETH Zurich, 2019). "What's so special about this structure is that ... there is no room in the narrow channels for water to form ice crystals, so it remains disordered even at extreme sub-zero temperatures. The lipids don't freeze either" (ETH Zurich, 2019). In any case, let us remember that in all the water-based lyotropic liquid crystals (Neto & Salinas, 2005), we have the presence of water confined in narrow channels.

Gibbs composite-system thermodynamics

As we can find told by Michael R. Landry, 2005, the thermoporometry is a measurement method of the pore size, obtained by means of the "melting or freezing point depression of a liquid confined in a pore". The depression is due to the "contribution of *surface curvature* to the phase-transition free energy". In the article by Landry, a specific section is discussing the "heating versus cooling experiments". There, it is stressed that it is important to distinguish the two measures, in heating and cooling, and also to distinguish the terms "supercooling" and "undercooling" used to "describe the delayed onset of liquid-solidification" (Landry, 2005). Supercooling is used to indicate the metastable liquid state below the equilibrium freezing temperature of the liquid, which is observed when the *porosity effect is absent*; for a supercooled liquid the freezing temperature is "not reproducible with any precision" (Landry, 2005). The undercooling is the presence of liquid below the equilibrium freezing temperature due solely to the *confinement in the pores*. In

this case, the freezing temperature is reproducible (Landry, 2005). In literature, we can find both mentioned and evaluated the melting and freezing point depression of temperatures.

Eq. 12 in the article by Landry is giving the relationship between the temperature depression ΔT and the pore size d is given as (note the approximation):

$$\Delta T \approx \frac{4 T_0 \gamma_{ls}}{d \rho_l H_f} \cos\theta \qquad (4)$$

Angle θ is given by Eq. 3 in Landry's discussion about liquid (mercury) intrusion porometry. The density is that of the liquid mass. Please consider the derivation of this equation in the Appendix of Landry's work. This equation is "*analogous* to the Gibbs–Thompson equation", the equation regarding the melting point depression for "small crystalline solids" (Landry, 2005). It is also noted that "a *layer of non-freezable liquid* usually exists along the walls of a porous material" (Landry, 2005).

As given by Landry, the melting point depression for a mesoconfined solid phase can be obtained from the Gibbs surface thermodynamics. In 2020, Janet Elliott has also discussed this thermodynamics required by composite materials, remembering that it is based on the work by J. W. Gibbs, "On the Equilibrium of Heterogeneous Substances", published in two parts in 1876 and 1878 respectively. Its applications are mainly in the fields of biotechnology and nanoscience, including the systems with interfaces, curved interfaces and multicomponent phases (Elliott, 2020).

Water in silica nanopores

Among the porous materials, mesoporous silica gained popularity in 1992 when it was disclosed a method to produce silica particles having inside a regular network of pores with hexagonal and cubic symmetries (Kresge et al., 1992, Beck et al., 1992). The method, proposed as based on a liquid-crystal 'templating' mechanism, is a form of modified Stöber process (Sparavigna, 2022). Most commonly used mesoporous silica particles are MCM-41 and SBA-15, both with hexagonal symmetric arrangement of pores.

Findenegg et al., 2008, considered the water freezing and melting in silica nanopores. The researchers give Gibbs-Thomson equation in the form:

$$T_p(R) - T_0 = -\frac{C}{R} \text{ with } C = \frac{2 T_0 \nu (\gamma_{WS} - \gamma_{WL})}{\Delta h_{SL}} \qquad (5)$$

Quantities γ_{WS}, γ_{WL} are the surface free energies per unit area of two interfaces, wall/solid and wall/liquid. Δh_{SL} is the enthalpy and ν the volume of the liquid or solid phase, "depending on which has the lower surface free energy against the wall" (Findenegg et al., 2008). The equation can be rewritten by means of the Young's equation:

$$\gamma_{WS} - \gamma_{WL} = \gamma_{SL} \cos\theta \qquad (6)$$

γ_{SL} is the interfacial tension of ice/water, θ represents the contact angle formed by the ice/water interface with the wall (Findenegg et al., 2008). Eq.5 gives a melting temperature in pores which can be depressed or elevated, depending on the difference between the surface energies. As stressed by Findenegg and coworkers, "in most cases the former situation $(\gamma_{WS} - \gamma_{WL} > 0)$ prevails, since liquids can adapt to rough pore walls better than crystalline solids". In the article by Findenegg et al. we can find also two wetting scenarios: the partial wetting case and the complete wetting case. For partial wetting, $\theta < 90°$, the solid phase is remaining "in direct contact with the wall up to the pore melting temperature"; in the case of the complete wetting, $\theta = 0°$, and due to a strong feeling of the pore wall for liquid, "a thin liquid-like layer starts to form at the solid/wall interface at a temperature well below" the pore melting temperature. "The

existence of such a premelted layer at the pore walls is not accounted for in the original Gibbs–Thomson relation" (Findenegg et al., 2008).

Using mesoporous silica materials MCM-41 and SBA-15 of well-known pore radius R, Findenegg and coworkers are fitting the data with the curve:

$$\Delta T_p(R)=\frac{C}{R-t} \qquad (7)$$

Forcing a fit with $t = 0$ is not possible for pore radii $R < 2$ nm. Therefore, the result is suggesting that the ice in the pores has a radius $R_S = R-t$, where t is the thickness of a liquid-like layer, when we are at the melting temperature.

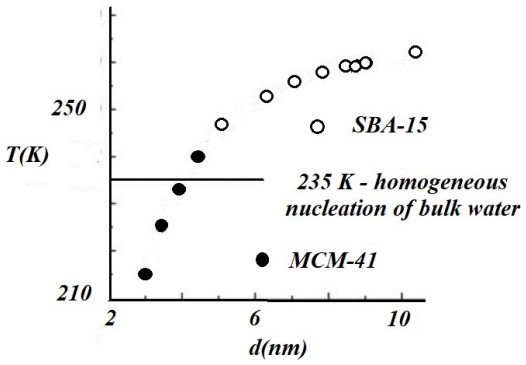

Fig. 1 - Effect of pore diameter d in nm, on the melting temperature of water in cylindrical pores of ordered MCM-41 and SBA-15, as given in the Figure 1 of the article by Findenegg et al., 2008.

In the discussion of their work, Findenegg and coworkers are mentioning the "open question" regarding "the transition from melting/freezing to some sort of glass transition of water as the pore size is reduced". In fact, it is given by experiments that the first-order phase transition vanishes in nanopores of MCM-41 (Findenegg et al., 2008). There are two effects to consider: the increasing disorder in the ice phase when the size of pores is reduced, and the increasing of the short-range order in the liquid phase at the low temperatures in narrow pores. "As a result, the local structure of ice and liquid water in the pores becomes more and more alike as the pore size decreases". Findenegg and coworkers note that X-ray and neutron diffraction analyses have given the ice in a defective form of ice with cubic features, rather than with hexagonal features. Further precise discussions of other experimental results are given by Findenegg and coworkers.

MCM-41, SBA-15 and PCMs

MCM-41 and SBA-15 are the hexagonal symmetry mesosilicas used by Findenegg and coworkers to study water. MCM-41 means Mobil Composition of Matter n.41, as being proposed by a Mobil Research team (Beck et al., 1992). The discovery of SBA-15, Santa Barbara n.15, is ascribed to the Galen D. Stucky Group in 1998 (Zhao et al., 1998). SBA-15 has a high specific surface area in a final material which is stable and displaying a high mechanical resistance (Galarneau et al., 2007, Benamor et al., 2012). In Roucher et al., 2019, it is stressed that the main feature of the materials is the presence of quite large pores, with respect to zeolites, which is consequently allowing even large molecules to diffuse. In the discussion by Vallet-Regí et al., 2022, SBA-15 is shown having a structure with pores arranged in hexagonal order, with micropores in the walls which are connecting the mesopores. Then SBA-15 is a micro-mesoporous silica material (Ojeda-López et al., 2021).

MCM-41 and SBA-15 are considered in the review about phase-change materials (PCMs) based on mesoporous silica given by Mitran et al., 2018. PCMs are substances absorbing or releasing large amounts of latent heat, when they go through a phase-change transition, i.e., from solid to liquid and vice versa. Mitran and coworkers remark that mesosilica MCM-41 and SBA-15 are the most commonly used mesoporous silica materials with hexagonal symmetry. Examples of mesoporous silica with cubic symmetries include MCM-48, SBA-16, KIT-6 and FDU-12 mesosilicas. The researchers are also stressing the existence of a layer wetting the surface of silica pores. This layer has liquid-like behavior even at temperatures "well below the melting point". The example proposed is water in 1.8 nm MCM-41 pores, where this layer remains liquid down to 21-26 K (the article mentioned by Mitran et al. is that by Juras et al., 2005). "The non-melting layer thickness, t, depends on the confined species, pore curvature and temperature" (Mitran et al., mentioning Liu et al., 2006, and Petrov et al., 2007). "The non-melting layer is typically one or two molecules thick for larger substances and up to four monolayers for smaller species, such as water or argon" (Mitran et al., mentioning Wallacher and Knorr, 2001).

We have in the "mesoporous silica-based heat storage materials", that the melting and crystallization points are different with respect to those of the bulk. "For mesoporous silica, the melting point is usually decreased with respect to bulk for all types of PCMs" (Mitran et al., 2018). In a confined phase with radius r, the melting temperature $T(r)$ turns out to be increased or reduced, when compared with the bulk melting temperature $T(\infty)$. The melting temperature change is given by Mitran et al., as:

$$T(\infty)-T(r)=-\frac{T(\infty)}{\Delta H_f}\frac{\alpha}{r}(V_l\gamma_l-V_s\gamma_s) \quad (8)$$

ΔH_f is the molar enthalpy of fusion, V_l, V_s and are the molar volumes of liquid and solid phases, γ_l, γ_s are the surface energies of the liquid and solid, α is a geometric parameter related to the pore geometry, which is 1 for cylinder and 2 for sphere. If the change in molar volume is negligible, it is assumed $V_m \approx V_l \approx V_s$ as the molar volume. If the liquid phase is wetting the solid, $\gamma_s - \gamma_l = \gamma_{sl}$ which is the surface tension of the solid-liquid interface. The equation previously given becomes:

$$T(\infty)-T(r)=-\frac{T(\infty)}{\Delta H_f}\frac{\alpha}{r}(V_m\gamma_{sl}) \quad (9)$$

Mitran and coworkers observe that the Gibbs-Thompson equation "has several important limitations". One of them is the above mentioned presence of a wetting layer at the silica surface. Moreover, the model does not consider other features at the pore surface, which can be the presence of defects or of different crystalline phases. The model "becomes unreliable for small pore sizes, usually below 3-7 nm" (Mitran et al., mentioning Liu, S. et al., 2016, Sterczyńska et al., 2014).

DSC, NMR, Cryo-NMR, FT-IR and Raman measurements

Jähnert et al., 2008, have considered the melting and freezing of water (H_2O, D_2O) in the silica nanopores of MCM-41, with diameters from 2.5 to 4.4 nm, studied by means of differential scanning calorimetry, DSC, and ^1H NMR cryoporometry. DSC resolved melting and freezing peaks for diameters down to 3.0 nm, "but not in 2.5 nm pores". The framework used by Jähnert and coworkers is given by the Gibbs–Thomson model, if the layer of nonfreezing water at the pore walls is considered. DSC measurements are giving hysteresis connected with phase transition. Hysteresis and melting enthalpy of water in the pores vanish about a pore diameter D* ≈ 2.8 nm. "It is concluded that D* represents a lower limit for first-order melting/freezing in the pores" (Jähnert et al., 2008). However, measurements by Spin Echo NMR show that "a transition from low to high mobility of water molecules takes place in all MCM-41 materials, including the one with 2.5 nm pores" (Jähnert et al., 2008). The transition temperature obtained by NMR is higher than that given by DSC. The difference becomes greater when the pore size decreases, so that "with decreasing pore size an

increasing fraction of the water molecules is situated in the first and second molecular layers next to the pore wall, and these molecules have slower dynamics than the molecules in the core of the pore" (Jähnert et al., 2008).

Confinement of water and solid–liquid phase transitions had been investigated by means of DSC and FT-IR measurements by Kittaka et al., 2006. Enthalpy changes upon melting in MCM-41 and SBA-15 mesosilica were determined as a function of pore size. They decrease with decreasing pore size. The melting point decreased almost monotonically with a decrease in pore size. The measurements tell that "the simple Gibbs–Thomson relation, i.e., a linear relation between the melting point change and the inverse pore size, is limited to the range not far from the melting point of bulk water" (Kittaka et al., 2006). According to Kittaka and coworkers, the FT-IR measurements tell that "the decrease in enthalpy change and interfacial free energy change with decreasing pore size reflect the *similarity* of the structures of both liquid and solid phases of water in smaller pores at lower temperatures."

Neutron scattering studies of water molecules in MCM-41 had been performed by Takahara et al., 1999. The measurement was performed on three water-filled MCM-41 samples, possessing different pore sizes. The temperature range was from 200 to 300 K. The analysis of spectra was based on a model considering two motions of molecules: rotational and translational diffusion motions. Regarding diffusion, the molecules in MCM-41 are less mobile than in bulk water. The mobility is decreased according to the narrowing of pore size. Moreover, the "growth of the hydrogen-bond network of water is hindered in a confined space by surface field" (Takahara et al., 1999). In the following table, some results are given as proposed by Takahara and coworkers, regarding the three samples.

Sample	specific surf. area $m^2 \cdot g^{-1}$	pore radius (nm)	Na content / ppm	Melting temp (K)
C10	1096	1.07	180	_
C14	1300	1.42	160	221
C18	837	1.87	100	242

A peak due to the melting of water in the pores of silica was observed for C14 and C18 samples. No peak is displayed by C10 sample. The peak temperatures are given, with other data, in the table. The melting temperature of C14 and C18 are "obeying apparently the Gibbs−Thomson equation. When the Gibbs−Thomson equation is applied to C10 sample, the deduced melting temperature is 193 K. However, the water in the C10 sample did not freeze down to 173 K" (Takahara et al., 1999).

Wang et al., 2019, have investigated water in mesopores by means of solid state NMR. The researchers analyzed the co-existing of solid ice and interfacial water within MCM-41 and SBA-15 "below the Gibbs-Thomson transition temperature" by means of Cryo-NMR, NMR spin-diffusion and NMR spectral analysis. The "difference of the ice cores and interfacial water layers in MCM-41 and SBA-15 is unveiled" (Wang et al., 2019). The typical mesoporous MCM-41 and SBA-15 have been chosen due to their mesoporous framework with well-defined cylinder geometry and a narrow pore size distribution. Wang and coworkers measured the thickness d_I of the interfacial water layer. "Our study demonstrates that below the GT [Gibbs-Thomson] transition temperature SBA-15 has a bigger d_i than that of MCM-41, although the structures in the interfacial layers are similar in both materials" (Wang et al., 2019).

From their data analysis the researchers concluded that, reasonably, in the interfacial region of SBA-15 , there is an extra monolayer of mobile water, with respect to the interfacial zone of MCM-41. "The measured thickness of the interfacial layers in SBA-15 was 2.5–3.0 Å thicker than that of MCM-41. ... The different thickness of the interfacial layer can be attributed to the different contact surfaces, therefore interfacial effects in MCM-41 and SBA-15" (Wang et al., 2019).

Erko et al., 2011, have investigated the confinement of water by Raman scattering. Pore diameters of MCM-41 and SBA-15 range from 2.0 to 8.9 nm. About Raman, "liquid–solid phase transition temperature of water in confinement can be determined by the analysis of the mode contribution in the OH-stretching region" (Erko et al., 2011). Down to 3 nm pore size, the results are consistent with the modified Gibbs-Thomson equation, "with a nonfreezable water layer of 0.6 nm (about two monolayers) close to the pore walls" (Erko et al., 2011). Again, it is told in the article that, if the pore size is 2.5 nm or smaller, a first-order phase transition is not displayed, and this is in agreement with DSC measurements. The data coming from Raman measurements suggest the existence in the small pores of "two spatially separated water phases": the "nonfreezable wall layer and a structurally different water phase in the core of the pores" (Erko et al., 2011). The researchers evidences that the tetrahedral hydrogen-bonded network of molecules is present only in the core part of pores. In the case of the weakest confinement, that is in the framework with pore diameter of 8.9 nm, "the core water is shown to be compatible with crystalline ice with a *spectral fingerprint* similar to bulk ice" (Erko et al., 2011). In the case of a strong confinement , that is a diameter of 2.0 nm, "the core water shows a spectral fingerprint identical to low-density *amorphous* ice, and there is a gradual transition between these two extremes" (Erko et al., 2011).

Hybrid ice

Deschamps et al., 2011, considered the water melting/freezing processes in the case of a strongly hydrophobic confinement in mesopores. The researchers found the persistence of the liquid state, "down to temperatures much lower than in the bulk and in hydrophilic materials of comparable sizes", so that Deschamps and coworkers defined the "thermodynamic limit for the melting/crystallization of water".

Moore, et al., 2012, uses molecular dynamics simulations to determine the behavior of confined ice and water as a function of temperature for cylindrical nanopores. In the simulations, the interaction between walls and water was ranging from "strongly hydrophilic to very hydrophobic". The simulations by Moore et al. show that the ice in the nanopores is "a hybrid ice I with stacks of cubic and hexagonal layers". Of course, the melting temperature is dependent on the radius of the pore "but rather insensitive to the hydrophilicity of the pore surface". Moore and coworkers have also considered the "premelted liquid layer". It exists in the confined ice down to 50 K below the melting temperatures of the ice confined in the nanopores. "The fraction of water in the premelted liquid layer decreases with increasing hydrophobicity of the pore wall, but it does not vanish even for the most hydrophobic nanopores" (Moore et al., 2012). Ice I_C is a metastable cubic crystalline ice, where the oxygen atoms are arranged in a diamond-like structure. It is present between 130 and 220 K and can exist up to 240 K (Murray & Bertram, 2006, Murray, 2008), when it turns into normal I_H hexagonal crystalline ice.

Water in three regimes

Xia et al., 2020, consider the freezing of water layer-by-layer in SBA-15 and SBA-16. The mesosilica SBA-16 has highly ordered 3-D cubic structure. In the introduction of their article, Xia and coworkers tell that the water confined in nanometer-sized pores, that is in "nanoarchitected solids", has a noticeably different behavior when compared to the bulk water. And also: "water ... displays pronounced dynamical heterogeneity under nanoconfinement and freezes in a stepwise fashion" (Xia et al., 2020). Moreover, the experimental observations of the nanoconfined water suggested a "fragile-to-strong liquid-liquid

polyamorphic transition en route to freezing" (Xia et al., 2020). As given by Diana Lutz, 2014, strong liquids seem to be able of forming good glasses, ignoring "inducements to crystallize". Fragile liquids are generally "bad glass formers". Faraone et al., 2004, assert that at about 225 K, a fragile-to-strong liquid–liquid transition exists, in the deeply supercooled confined water.

After mentioning the Gibbs-Thomson effect, Xia et al. continue asserting that, in spite of fact that the freezing/melting behavior has been studied "extensively in the past, the nature of the dynamics of nanoconfined water during the solidification process remains quite controversial" (Xia et al., 2020). The majority of the studies give the presence of three "spatial regimes" for the water in porous silica with pore sizes ranging from 2 nm to 20 nm. Xia and coworkers summarize the three regimes in the following manner. The "first regime" is a monolayer of about thickness 0.3 nm. This is made of the water molecules that are bound to the pore wall. The molecules can "perform restricted rotational motion". "This layer is believed to remain unfrozen even down to ~190 K" (Xia et al., 2020). Then we find a shell of water, where molecules "still remain strongly structured" according to the pore walls up to a distance of about 1 nm. The mobility of this water is "significantly lower, while its density is higher, compared to that of bulk water" (Xia et al., 2020). This shell of water is characterized by a density layering. The “core” region is that beyond 1 nm from the pore wall. The water in the core is considered to be like that of the bulk water. The consequence of the model made by the three regimes is that, upon cooling, "the core region will freeze first, followed by the shell region and thus, the latter will display a stronger effect of spatial confinement compared to the former" (Xia et al., 2020). Probably there is a gradual change from the pore wall to its center (Xia et al., 2020). This is in agreement with DSC measurements. Nuclear magnetic resonance (NMR) spectroscopy shows the presence of "heterogeneous dynamics with a bimodal behavior characterized by the coexistence of a relatively immobile and a highly mobile fraction of molecules below the DSC freezing point" (Xia et al., 2020, mentioning Sattig and Vogel, 2014). The coexistence of mobile and immobile molecules seems to be consistent "with a gradual variation of the melting point across the core-shell boundary region" (Xia et al., 2020). Xia and coworkers are proposing in their article a systematic study of water confined SBA-15, SBA-16 and VycorTM. The researchers conclude that "the gradual “layer-by-layer” freezing model" is consistent with experiments and "can also explain the recently reported observation of an apparent fragile-to-strong dynamic crossover in nanoconfined water" (Xia et al., 2020).

Cashmere, cotton and cellulose fibers

We have seen the large use of mesosilica particles, in particular MCM-41 and SBA-15, to study the behavior of water in them. However, water in pores can be used as a probe for several applications. For instance, Zhan et al., 2021, have used water to investigate a natural protein fiber, the cashmere. "In the textile manufacturing processes", water is used as solvent for dyestuffs and finishing substances. It is also "a transportation medium for those infiltrates to the interior of fabrics" (Zhan and coworkers mentioning Mao et al., 2014). As explained by Zhan and coworkers, the interaction of water with keratin is relevant for the features of cashmere macromolecules, besides acting in the control of the mechanical properties of fibers and for the stability of cashmere fabrics during the finishing process. Understanding the interactions of water with fibers is therefore fundamental to improve the wearing comfort of textiles.

Besides DSC, the dynamic water vapor sorption (DVS) can be used to determine the pore size distribution according to the Gibbs−Thomson effect. The combined measurements have been made for cashmere. "Based on the unfreezable threshold and hygroscopic properties, different types of water in cashmere and the interaction between water and fibers were investigated" (Zhan et al., 2021). In cashmere, the pore size distribution tell that pores were less than 60 nm in diameter.

Mao et al., 2014, have considered the pore properties, such as the specific surface area and the average pore size, of cotton fibers. Water was used as a probe in DSC measurements based on the Gibbs–Thomson effect. Mao and coworkers found that "larger pores changed in size with the change of moisture ratio prior to

smaller pores in both wetting and drying of cotton fibers" (Mao et al., 2014). This information can be relevant for dyeing processes. In this manner, besides improving the fabric surface performance, "large amounts of water and energy could be saved by low add-on technology" (Mao et al., 2014).

Let us also add to the these two applications, the one proposed by Park et al., 2006. It is a research that we have previously mentioned. Park and coworkers evaluated the changes in pore size distribution of the cellulose fibers during the drying process. DSC measurements have been made by an isothermal step melting procedure.

In carbon nanopores

Florent et al., 2021, investigated the melting of water in carbon nanopores and the role of their surface chemistry. The shift of a water melting point was observed under distinctive surface chemistry. In the prepared carbons, the size of pores was similar but the chemistry differed. "As expected for carbon materials, the melting point of water decreased compared to that in the bulk ... Nevertheless, that decrease was smaller for carbons of most acidic surface and thus for those attracting water than for carbons of hydrophobic surface" (Florent et al., 2021).

Jazdzewska et al., 2011, report results on the structure and melting of ice confined in multi-walled carbon nanotubes and in the ordered mesoporous carbon CMK-3. This mesoporous carbon is the replica of SBA-15 as silica template. Due to the framework of the template, the carbon replica CMK-3 is made of carbon rods joined by smaller side-branches, so that there are mesopores of averaged size 4.9 nm and micropores of 0.6 nm. The researchers used neutron diffraction and DSC measurements to study the confined ice and the transition temperature. "For D_2O in CMK-3 we find evidence of the existence of nanocrystals of cubic ice and ice IX; the diffraction results also suggest the presence of ice VIII, although this is less conclusive. We find evidence of cubic ice in the case of the carbon nanotubes" (Jazdzewska et al., 2011). Jazdzewska and coworkers stress that, for the bulk water, the cubic ice is observed at temperatures below 170 K, and ice VIII and IX at pressures of hundreds or thousands of MPa. "These phases appear to be stabilized by the confinement" (Jazdzewska et al., 2011).

Domin et al., 2016, inserted deionized water into the pores of the ordered carbon of CMK-3 and CMK-8. DSC has been used to find the melting transition temperature of the confined ice. The wide-angle X-ray scattering was used to study the ice formed inside the carbon mesopores. The temperature range of measurements was from 173 K to the pore melting point. XRD displayed the presence of features related to both hexagonal I_h and cubic I_c ice, below the melting point. "The structure of the confined ice corresponds to disordered stacking ice layers, ice I_{sd}" (Domin et al, 2016).

For what is regarding the fluid-wall interaction, Sliwinska-Bartkowiak et al., 2018, had provided experimental measurements in carbon and silica nanopores. Phase transitions of H_2O, D_2O and $C_6H_5NO_2$ confinement in pores of different inner diameter (range of 2.2-7.5 nm) are given. Sliwinska-Bartkowiak and coworkers show that melting temperatures of the confined system "decrease relative to the bulk for weaker fluid-wall than fluid-fluid interaction (silica glasses) and increase in the case of stronger fluid-wall interaction (carbon pores)" (Sliwinska-Bartkowiak et al., 2018).

Let us consider also the research by Morishige et al., 2010, on the effect of pore shape on water freezing and melting temperatures, by means of X-ray diffraction patterns. The water was confined in ordered mesoporous silicas, possessing a thin carbon films on the wall of the pores and in inverse carbon replicas. The researchers observed that melting temperatures have a good correlation with capillary condensation pressure of nitrogen at 77 K. "The melting point depression of the pore ice revealed an almost linear relationship with ln(p0/p) of the capillary condensation pressure of nitrogen at 77 K for various pores of different sizes and shapes" (Morishige et al., 2010). According to Morishige and coworkers, the result is

suggesting that $\ln(p_0/p)$ for capillary condensation of nitrogen at 77 K can provide a good measure of pore size, "irrespective of the pore shapes".

Biochar

Biochar is a fine-grained residue of pyrolysis of biomass, obtained by thermochemical decomposition at moderate temperatures (350–700°C) under oxygen-limiting conditions (Brassard et al., 2019). Besides biochar proper, liquid (bio-oil) and gas (syngas) products are obtained from the thermal decomposition (Han & Kim, 2008, Ok et al., 2018, Bartoli et al., 2020, Giorcelli et al., 2021). The principal use of biochar is as amendment in agricultural soils, because of its high carbon content, stability, porosity and surface area (Brassard et al., 2019, Ok et al., 2015). Since biochar exhibits high compatibility with cement, asphalt and polymer, it is suitable for several non-soil applications (Bartoli et al., 2020, 2022, Tan et al., 2021, Zhao et al., 2014, Zhang et al., 2018, Das et al., 2021, Lepak-Kuc et al., 2021).

Being largely used to improve the soil water holding capacity, biochar has been investigated by Bikbulatova et al., 2018, to understand the water behavior in it. The biochar used by the researchers was produced from peanut shell and palm kernel shell. "Water holding capacity and water adsorption rate showed a direct correlation with micropore volume of biochar, suggesting that physical structure of biochar played a key role during interaction with water" (Bikbulatova et al., 2018).

Several previous references are mentioned by Bikbulatova and coworkers about the interaction of soil moisture retention capacity and biochar; in particular Sun and Lu, 2014, reported that the use of biochar in soil is increasing the water retention and consequently the quantity of water available for plants, because it is increased the total porosity of soil. Also Ulyett et al., 2014, investigated the effect of biochar on the water retention of sandy loam soils, attributing the moisture retention to the porous biochar.

"Although it is generally agreed that biochar has a high water holding capacity, the *exact interaction* between water and biochar ... is not fully understood" (Bikbulatova et al., 2018). However, researches exist about water in porous media and Bikbulatova and coworkers are mentioning those about water in silica (Findenegg et al., 2008, Jähnert et al., 2008), low-rank coals (Yu et al., 2013, Tahmasebi et al., 2014), and lignite char (Nwaka et al., 2016). The literature given previously shows that different types of water is present in the porous medium of low-rank coals and lignite (Bikbulatova et al., 2018, and references therein). The types are: “freezable free water” (FFW), “freezable-bound water” (FBW), and “non-freezable bound water” (NFW). FFW is that present at the particle surface and in the large pores of biochar, but FBW is condensed in micropores (Mraw and O'Rourke, 1982). "It has been reported that meso and macropores in biochar act as the passageways of water to micropores, where most of the adsorption takes place" (Bikbulatova et al., 2018, Pastor-Villegas et al., 2006, Asai et al., 2009, Rouquerol et al., 1999).

In 2018, the different types of water and the effect of physical and chemical structure of biochar on moisture content - according to Bikbulatova and coworkers - was not given in literature. The purpose of research work was therefore that of investigating these features. By means of DSC measurements, Bikbulatova and coworkers observed two types of freezable water, the freezable free water (FFW) and the freezable bound water (FBW). "The phase transition temperature of freezable bound water correlated well with pore size distribution of bio-chars. ... The difference between the total water content and the sum of FFW and FBW in samples suggested the presence of NFW in biochars. The presence of NFW was confirmed by low-temperature XRD analysis" (Bikbulatova et al., 2018).

The research used the modified Gibbs-Thomson equation, for pores with diameter less than 5 nm, to represent the phase transition temperature depression of FBW. Bikbulatova and coworkers consider the non-freezable water layer near the pore wall, assuming a thickness of two water layers. By means of DSC measurements, it has been observed that the amount of FFW and FBW in biochar "decreased with decreasing water content, accompanied by a monotonic increase in NFW". It is also concluded that "the

amount of FBW in bio-char samples showed a direct relationship with micropore volume of the samples, suggesting that this type of water is mainly present in smaller pores" (Bikbulatova et al., 2018).

Once again, as previously tressed in 2022, about biochar shape-stabilized phase-change materials, the role of micro-, meso- and macropores is fundamental to have a better picture of all the relevant features of biochar.

References

[1] Asai, H., Samson, B.K., Stephan, H.M., Songyikhangsuthor, K., Homma, K., Kiyono, Y., Inoue, Y., Shiraiwa, T., & Horie, T. (2009). Biochar amendment techniques for upland rice production in Northern Laos: 1. Soil physical properties, leaf SPAD and grain yield. Field crops research, 111(1-2), 81-84.

[2] Bartoli, M., Giorcelli, M., Jagdale, P., Rovere, M., & Tagliaferro, A. (2020). A review of non-soil biochar applications. Materials, 13(2), 261.

[3] Bartoli, M., Rosi, L., & Frediani, M. (2020). From Waste to Chemicals: Bio-Oils Production Through Microwave-Assisted Pyrolysis. In Production of Biofuels and Chemicals with Pyrolysis (pp. 207-231). Springer, Singapore.

[4] Bartoli, M., Arrigo, R., Malucelli, G., Tagliaferro, A., & Duraccio, D. (2022). Recent advances in biochar polymer composites. Polymers, 14(12), 2506.

[5] Beck, J. S., Vartuli, J. C., Roth, W. J., Leonowicz, M. E., Kresge, C. T., Schmitt, K. D., Chu, C. T. W., Olson, D. H., Sheppard, E. W., & McCullen, S. B. (1992). A new family of mesoporous molecular sieves prepared with liquid crystal templates. J. Am. Chem. Soc. 1992, 114, 10834−10843.

[6] Benamor, T., Vidal, L., Lebeau, B., & Marichal, C. (2012). Influence of synthesis parameters on the physico-chemical characteristics of SBA-15 type ordered mesoporous silica. Microporous and Mesoporous Materials, 153, 100-114.

[7] Bikbulatova, S., Tahmasebi, A., Zhang, Z., Rish, S. K., & Yu, J. (2018). Understanding water retention behavior and mechanism in bio-char. Fuel Processing Technology, 169, 101-111.

[8] Brassard, P., Godbout, S., Lévesque, V., Palacios, J. H., Raghavan, V., Ahmed, A., Hogue, R., Jeanne, T., & Verma, M. (2019). Biochar for soil amendment. In Char and carbon materials derived from biomass (pp. 109-146), Elsevier, 2019.

[9] Brun, M., Lallemand, A., Quinson, J. F., & Eyraud, C. (1977). A new method for the simultaneous determination of the size and shape of pores: the thermoporometry. Thermochimica acta, 21(1), 59-88.

[10] Cantor, B. (2020). The Equations of Materials. Oxford University Press. ISBN: 9780198851875, 0198851871

[11] Das, C., Tamrakar, S., Kiziltas, A., & Xie, X. (2021). Incorporation of biochar to improve mechanical, thermal and electrical properties of polymer composites. Polymers, 13(16), 2663.

[12] Deschamps, J., Audonnet, F., Brodie-Linder, N., Schoeffel, M., & Alba-Simionesco, C. (2010). A thermodynamic limit of the melting/freezing processes of water under strongly hydrophobic nanoscopic confinement. Physical Chemistry Chemical Physics, 12(7), 1440-1443.

[13] Domin, K., Chan, K. Y., Yung, H., Gubbins, K. E., Jarek, M., Sterczynska, A., & Sliwinska-Bartkowiak, M. (2016). Structure of ice in confinement: Water in mesoporous carbons. Journal of Chemical & Engineering Data, 61(12), 4252-4260.

[14] Elliott, J. A. (2020). Gibbsian surface thermodynamics. The Journal of Physical Chemistry B, 124(48), 10859-10878.

[15] Erko, M., Findenegg, G. H., Cade, N., Michette, A. G., & Paris, O. (2011). Confinement-induced structural changes of water studied by Raman scattering. Physical Review B, 84(10), 104205.

[16] ETH Zurich (2019). Water that never freezes. Science Daily. 10 April 2019. Link: www.sciencedaily.com/releases/2019/04/190410114117.htm.

[17] Fang, Q. R., Makal, T. A., Young, M. D., & Zhou, H. C. (2010). Recent advances in the study of mesoporous metal-organic frameworks. Comments on Inorganic Chemistry, 31(5-6), 165-195.

[18] Faraone, A., Liu, L., Mou, C. Y., Yen, C. W., & Chen, S. H. (2004). Fragile-to-strong liquid transition in deeply supercooled confined water. The Journal of chemical physics, 121(22), 10843-10846.

[19] Findenegg, G. H., Jähnert, S., Akcakayiran, D., & Schreiber, A. (2008). Freezing and melting of water confined in silica nanopores. ChemPhysChem, 9(18), 2651-2659.

[20] Florent, M., Rotnicki, K., Przybylska, N., Sliwinska-Bartkowiak, M., & Bandosz, T. J. (2021). Exploring the effect of surface chemistry in carbon nanopores on melting behavior of water. Carbon, 185, 252-263.

[21] Galarneau, A., Nader, M., Guenneau, F., Di Renzo, F., & Gedeon, A. (2007). Understanding the stability in water of mesoporous SBA-15 and MCM-41. The Journal of Physical Chemistry C, 111(23), 8268-8277.

[22] Giorcelli, M., Das, O., Sas, G., Försth, M., & Bartoli, M. (2021). A review of bio-oil production through microwave-assisted pyrolysis. Processes, 9(3), 561.

[23] Han, J., & Kim, H. (2008). The reduction and control technology of tar during biomass gasification / pyrolysis: an overview. Renewable and sustainable energy reviews, 12(2), 397-416.

[24] Jackson, C. L., & McKenna, G. B. (1990). The melting behavior of organic materials confined in porous solids, J. Chem. Phys., 93 (12), 9002–9011.

[25] Jähnert, S., Chávez, F. V., Schaumann, G. E., Schreiber, A., Schönhoff, M., & Findenegg, G. H. (2008). Melting and freezing of water in cylindrical silica nanopores. Physical Chemistry Chemical Physics, 10(39), 6039-6051.

[26] Jazdzewska, M., Śliwinska-Bartkowiak, M.M., Beskrovnyy, A.I., Vasilovskiy, S.G., Ting, S.W., Chan, K.Y., Huang, L., & Gubbins, K.E. (2011). Novel ice structures in carbon nanopores: pressure enhancement effect of confinement. Physical Chemistry Chemical Physics, 13(19), 9008-9013.

[27] Juras, B., Martynas, K., Jan, M., Georg, V., Winfried, B., Venkatesan, U., Martin, H., & Andreas, P. (2005). Broadband dielectric spectroscopy of water confined in MCM-41 molecular sieve materials: low-temperature freezing phenomena. J. Phys.: Condens. Matter, 17, 2843.

[28] Kittaka, S., Ishimaru, S., Kuranishi, M., Matsuda, T., & Yamaguchi, T. (2006). Enthalpy and interfacial free energy changes of water capillary condensed in mesoporous silica, MCM-41 and SBA-15. Physical Chemistry Chemical Physics, 8(27), 3223-3231.

[29] Kresge, C. T., Leonowicz, M. E., Roth, W. J., Vartuli, J. C., & Beck, J. S. (1992). Ordered mesoporous molecular sieves synthesized by a liquid-crystal template mechanism. Nature, 359, 710−712.

[30] Landry, M. R. (2005). Thermoporometry by differential scanning calorimetry: experimental considerations and applications. Thermochimica acta, 433(1-2), 27-50.

[31] Lepak-Kuc, S., Kiciński, M., Michalski, P. P., Pavlov, K., Giorcelli, M., Bartoli, M., & Jakubowska, M. (2021). Innovative Biochar-Based Composite Fibres from Recycled Material. Materials, 14(18), 5304.

[32] Liu, E., Dore, J. C., Webber, J. B. W., Khushalani, D., Jähnert, S., Findenegg, G. H., & Hansen, T. (2006). Neutron diffraction and NMR relaxation studies of structural variation and phase transformations for water/ice in SBA-15 silica: I. The over-filled case. J. Phys.: Condens. Matter, 18, 10009.

[33] Liu, S., Ma, G., Xie, S., Jia, Y., Sun, J., & Jing, Y. (2016). Diverting the phase transition behaviour of adipic acid via mesoporous silica confinement. RSC Adv. 2016, 6, 111787-111796.

[34] Lutz, D. (2014). Experiments explain why some liquids are 'fragile' and others are 'strong. Available at https://source.wustl.edu/2014/08/experiments-explain-why-some-liquids-are-fragile-and-others-are-strong/

[35] Mao, Z., Yu, H., Wang, Y., Zhang, L., Zhong, Y., & Xu, H. (2014). States of water and pore size distribution of cotton fibers with different moisture ratios. Industrial & Engineering Chemistry Research, 53(21), 8927-8934.

[36] Mitran, R. A., Berger, D., & Matei, C. (2018). Phase change materials based on mesoporous silica. Current Organic Chemistry, 22(27), 2644-2663.

[37] Moore, E. B., Allen, J. T., & Molinero, V. (2012). Liquid-ice coexistence below the melting temperature for water confined in hydrophilic and hydrophobic nanopores. The Journal of Physical Chemistry C, 116(13), 7507-7514.

[38] Morishige, K., Yasunaga, H., & Matsutani, Y. (2010). Effect of pore shape on freezing and melting temperatures of water. The Journal of Physical Chemistry C, 114(9), 4028-4035.

[39] Mraw, S. C., & O'Rourke, D. F. (1982). Water in coal pores: the enthalpy of fusion reflects pore size distribution. Journal of Colloid and Interface Science, 89(1), 268-271.

[40] Murray, B. J., & Bertram, A. K. (2006). Formation and stability of cubic ice in water droplets. Physical Chemistry Chemical Physics, 8(1), 186-192.

[41] Murray, B. J. (2008). Enhanced formation of cubic ice in aqueous organic acid droplets. Environmental Research Letters, 3(2), 025008.

[42] Nakamura, K., Hatakeyama, T., & Hatakeyama, H. (1981). Studies on bound water of cellulose by differential scanning calorimetry. Textile Research Journal, 51, 607–613.

[43] Neto, A. M. F., & Salinas, S. R. (2005). The physics of lyotropic liquid crystals: phase transitions and structural properties (Vol. 62). OUP Oxford.

[44] Nopens, M., Sazama, U., König, S., Kaschuro, S., Krause, A., & Fröba, M. (2020). Determination of mesopores in the wood cell wall at dry and wet state. Scientific Reports, 10(1), 1-11.

[45] Nwaka, D., Tahmasebi, A., Tian, L., & Yu, J. (2016). The effects of pore structure on the behavior of water in lignite coal and activated carbon. Journal of colloid and interface science, 477, 138-147.

[46] Ojeda-López, R., Domínguez-Ortiz, A., Felipe, C., Cervantes-Uribe, A., Pérez-Hermosillo, I. J., & Esparza-Schulz, J. M. (2021). Isosteric enthalpy behavior of CO2 adsorption on micromesoporous materials: carbon microfibers (CMFs), SBA-15, and amine-functionalized SBA15. Journal of Composites Science, 5(4), 102

[47] Ok, Y. S., Uchimiya, S. M., Chang, S. X., & Bolan, N. (Eds.). (2015). Biochar: Production, characterization, and applications. CRC press.

[48] Ok, Y. S., Tsang, D. C., Bolan, N., & Novak, J. M. (Eds.). (2018). Biochar from biomass and waste: fundamentals and applications. Elsevier.

[49] Park, S., Venditti, R. A., Jameel, H., & Pawlak, J. J. (2006). Changes in pore size distribution during the drying of cellulose fibers as measured by differential scanning calorimetry. Carbohydrate polymers, 66(1), 97-103.

[50] Pastor-Villegas, J., Pastor-Valle, J. F., Rodríguez, J. M., & García, M. G. (2006). Study of commercial wood charcoals for the preparation of carbon adsorbents. Journal of analytical and applied pyrolysis, 76(1-2), 103-108.

[51] Petrov, O. V., Vargas-Florencia, D., & Furó, I. (2007). Surface Melting of Octamethylcyclotetrasiloxane Confined in Controlled Pore Glasses: Curvature Effects Observed by 1H NMR. The J. Phys. Chem. B, 111, 1574-1581

[52] Roucher, A., Bentaleb, A., Laurichesse, E., Dourges, M. A., Emo, M., Schmitt, V., Blin, J. L. & Backov, R. (2018). First macro-mesocellular silica SBA-15-Si (HIPE) Monoliths: conditions for obtaining self-standing materials. Chemistry of Materials, 30(3), 864-873.

[53] Rouquerol, F., Rouquerol, J., & Sing, K. (1999). Adsorption by active carbons. Adsorption by Powders and Porous Solids: Principles, Methodology and Applications. Academic Press, London.

[54] Salamon, D. (2014). Advanced ceramics. In Advanced ceramics for dentistry (pp. 103-122). Butterworth-Heinemann.

[55] Salvati Manni, L., Assenza, S., Duss, M., Vallooran, J.J., Juranyi, F., Jurt, S., Zerbe, O., Landau, E.M., & Mezzenga, R. (2019). Soft biomimetic nanoconfinement promotes amorphous water over ice. Nature Nanotechnology, 14(6), 609-615.

[56] Sattig, M., & Vogel, M. (2014). Dynamic crossovers and stepwise solidification of confined water: A 2H NMR study. The journal of physical chemistry letters, 5(1), 174-178.

[57] Sing, K. S. (1991). Characterization of porous solids: An introductory survey. In Studies in Surface Science and Catalysis (Vol. 62, pp. 1-9). Elsevier.

[58] Sliwinska-Bartkowiak, M., Jazdzewska, M., Domin, K., & Gubbins, K. E. (2018). Effect of confinement on melting in nanopores. In Spin Orbitronics and Topological Properties of Nanostructures: Lecture Notes of the 12th International School on Theoretical Physics (pp. 140-155).

[59] Sparavigna, A. C. (2022). Lyotropic liquid crystals as templates for mesoporous silica materials. SSRN Electronic Journal. DOI: 10.2139/ssrn.4285677

[60] Sparavigna, A. C. (2022). Wood and Delignified Wood for Shape-Stabilized Phase-Change Materials in Application to Thermal Energy Storage. SSRN Electronic Journal. DOI: 10.2139/ssrn.4318007

[61] Sparavigna, A. C. (2022). Biochar Shape-Stabilized Phase-Change Materials for Thermal Energy Storage. SSRN Electronic Journal. DOI: 10.2139/ssrn.4310141

[62] Sterczyńska, A., Deryło-Marczewska, A., Śliwińska-Bartkowiak, M., Piotrowska, J. Z., Jarek, M., & Domin, K. (2014). Phase transitions of octamethylcyclotetrasiloxane confined inside aluminosilicate and silicate nanoporous matrices. J. Therm. Anal. Calorim. 118, 263-276.

[63] Sun, F., & Lu, S. (2014). Biochars improve aggregate stability, water retention, and pore-space properties of clayey soil. Journal of Plant Nutrition and Soil Science, 177(1), 26-33.

[64] Tahmasebi, A., Yu, J., Su, H., Han, Y., Lucas, J., Zheng, H., & Wall, T. (2014). A differential scanning calorimetric (DSC) study on the characteristics and behavior of water in low-rank coals. Fuel, 135, 243-252.

[65] Takahara, S., Nakano, M., Kittaka, S., Kuroda, Y., Mori, T., Hamano, H., & Yamaguchi, T. (1999). Neutron scattering study on dynamics of water molecules in MCM-41. The Journal of Physical Chemistry B, 103(28), 5814-5819.

[66] Tan, K. H., Wang, T. Y., Zhou, Z. H., & Qin, Y. H. (2021). Biochar as a partial cement replacement material for developing sustainable concrete: An overview. Journal of Materials in Civil Engineering, 33(12), 03121001.

[67] Ulyett, J., Sakrabani, R., Kibblewhite, M., & Hann, M. (2014). Impact of biochar addition on water retention, nitrification and carbon dioxide evolution from two sandy loam soils. European Journal of Soil Science, 65(1), 96-104.

[68] Vallet-Regí, M., Schüth, F., Lozano, D., Colilla, M., & Manzano, M. (2022). Engineering mesoporous silica nanoparticles for drug delivery: where are we after two decades?. Chemical Society Reviews, 51, 5365-5451

[69] Wallacher, D., & Knorr, K. (2001). Melting and freezing of Ar in nanopores. Phys. Rev. B, 63, 104202.

[70] Wang, J., Xue, H., Zhou, B., Yao, Y. F., & Hansen, E. W. (2019). Interfacial water in mesopores and its implications to the surface features–A solid state NMR study. Applied Surface Science, 484, 1154-1160.

[71] Xia, Y., Cho, H., Deo, M., Risbud, S. H., Bartl, M. H., & Sen, S. (2020). Layer-by-Layer freezing of nanoconfined water. Scientific reports, 10(1), 5327.

[72] Yu, J., Tahmasebi, A., Han, Y., Yin, F., & Li, X. (2013). A review on water in low rank coals: The existence, interaction with coal structure and effects on coal utilization. Fuel Processing Technology, 106, 9-20.

[73] Zhan, L., Li, Y., Ji, F., & Wang, N. (2021). Analysis of states of water in cashmere fibers and utilizing water as molecular probe for pore size distribution. Polymer Testing, 101, 107285.

[74] Zhang, Y., He, M., Wang, L., Yan, J., Ma, B., Zhu, X., Ok, S. Y., Mechtcherine, V., & Tsang, D. C. (2022). Biochar as construction materials for achieving carbon neutrality. Biochar, 4(1), 1-25

[75] Zhao, D., Feng, J., Huo, Q., Melosh, N., Fredrickson, G. H., Chmelka, B. F., & Stucky, G. D. (1998). Triblock copolymer syntheses of mesoporous silica with periodic 50 to 300 angstrom pores. science, 279(5350), 548-552.

[76] Zhao, S., Huang, B., Shu, X., & Ye, P. (2014). Laboratory investigation of biochar-modified asphalt mixture. Transportation Research Record, 2445(1), 56-63.

[77] Zhong, X., & Ma, E. (2022). A novel approach for characterizing pore size distribution of wood cell wall using differential scanning calorimetry thermoporosimetry. Thermochimica Acta, 718, 179380.